Thrust to Weight Improvement of JetCat P100-RX Turbojet Engine

Thomas Coulon, Riley Johnson, Lauren Jones, Michael Mines, Grant Schumacher, and Colton Swart
Mechanical & Aerospace Engineering, Oklahoma, Stillwater, 74075

The purpose of the presented design is to improve the thrust-to-weight ratio of the JetCat P100-RX small turbojet engine, a project sponsored by the Air Force Research Laboratory. This project is a year-long endeavor ending with a competition at the Wright-Patterson Air Force Base in Dayton, Ohio. The primary challenge is to increase thrust with minimal increase in weight. Several solutions were considered such as nozzle geometry optimization, exit guide vane addition, and material improvement. The final design included the optimized nozzle geometry configured with seven exit guide vanes with leading edges oriented 10-degrees into the exhaust flow. This new nozzle was additively manufactured in titanium to reduce weight and mitigate deformation from high exhaust gas temperatures. An inlet cowling of the original geometry was fabricated from foam to reduce weight. Finally, a new battery was substituted to reduce additional weight. The improved nozzle resulted in a thrust increase of 23%, and the material and battery improvements resulted in a weight reduction of 8%, leading to an overall thrust-to-weight improvement of 32%. The thrust-to-weight ratio was improved from 6.64 to 8.75.

Nomenclature

F	=	uninstalled thrust
$\dot{m}$	=	mass flow rate of air
g_c	=	proportionality constant
c_p	=	constant pressure specific heat
γ	=	specific heat ratio
P_t	=	total pressure
P	=	static pressure
T_t	=	total temperature
M	=	Mach Number
π	=	total pressure ratio
η	=	component efficiency
f	=	fuel/air ratio

I. Introduction

The purpose of this year-long project, sponsored by the Air Force Research Laboratory Aerospace Propulsion Outreach Program (APOP), is to increase the JetCat P100-RX turbojet thrust-to-weight ratio. The project is a competition which includes participating student teams from more than ten universities and will conclude at Wright-Patterson Air Force Base in Dayton, Ohio. The competition will include an engine run for one minute at maximum throttle, obtaining a time-averaged thrust. The current published thrust-to-weight ratio is 9.4 (not including the battery) with a maximum reported thrust of the engine is 22 lbf. The original weight of the engine is 1080 grams. The engine is shown in Figure 1 with specifications provided by the manufacturer. Many alternatives were considered to improve

thrust-to-weight ratio, while factoring in time, budget, and experience of the team. Options deemed viable were analyzed and implemented to improve engine capability.

Parameter	English	Metric
Max Thrust	22.48 lb	100 N
Mass	2.38 lb	1.08 kg
EGT	1292 °F	720 °C
EGV	1425 ft/s	434 m/s
Pressure Ratio	2.9	2.9
Mass Flow	0.64 lb/s	0.29 kg/s
Fuel Consumption	0.014 lb/s	0.0064 kg/s

Figure 1. JetCat P100-RX Turbojet (left) and Manufacturer Specifications (right)

II. Design Alternatives

Design alternatives that were considered generally included: increased mass flow rate through the engine, re-design of turbomachinery, afterburner, inlet and nozzle geometries, and material selection. The uninstalled thrust equation shown below indicates that increased mass flow rate and exhaust velocity contribute to improved thrust; manipulating the identified two variables is the focus of the project.

$$F = \frac{(\dot{m}_0 + \dot{m}_f)V_9 - \dot{m}_0 V_0}{g_c}$$

Equation 1

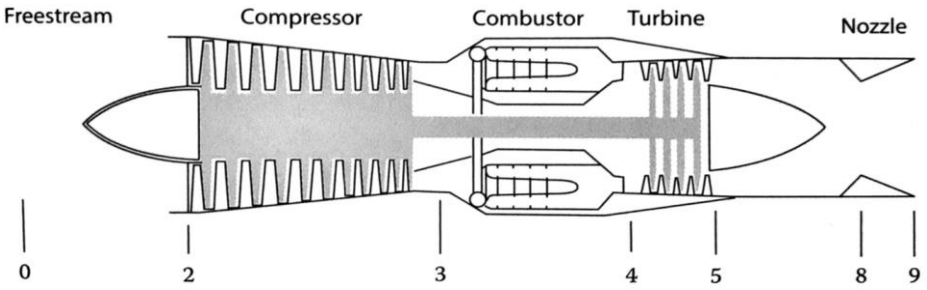

Figure 2. Turbojet Station Numbers[1]

A. Increased Fuel Mass Flow Rate

By increasing the fuel mass flow rate into the combustion chamber, the overall mass flow rate of the engine would increase, which in turn increases thrust. This increase is shown in the overall thrust equation by the m_{dot} terms on the right side of the equation: as m_{dot} increases, thrust increases.

To increase the fuel mass flow rate, the fuel pump for the engine could be reprogrammed to increase by a specified amount. However, the combustion process sets some limits on the values of the fuel to air ratio. In operation, there is a maximum burner exit temperature, Tt4, which is determined by material limits. If the engine is operated at a higher temperature than the maximum rated temperature, the burner and turbine could be damaged. Furthermore, this higher fuel-to-air ratio could quench the flame in the burner, having a detrimental effect on operability of the engine. The amount of fuel that was needed to create a significant increase in thrust was calculated and found to be too high for the combustor to hold a flame. For these reasons, increasing the fuel mass flow rate into the engine was not pursued for this design.

B. Water Injection

Using a spray device to inject water into the inlet of the engine, the overall mass flow rate through the engine can be increased, increasing thrust by the same method discussed in Part A. The same evaporation enthalpy will allow a higher mass flow in the intake, and thus, a higher mass flow in the combustion chamber can be achieved, resulting in more thrust. However, the fuel in the combustion chamber must also be fully evaporated for effective combustion, which takes more time and energy. If not, the flame could once again be quenched, this time due to the cooling of the flow. Lastly, the weight added from the fuel flow system and water tank would be detrimental to the thrust-to-weight ratio.

C. Turbomachinery

Figure 3 represents a Temperature-Entropy diagram for a turbojet engine. An increased compressor pressure ratio could be accomplished by modifying the compressor. This change could lead to an improved thermal efficiency, however, if the burner temperature does not change, this change would limit the design on the compressor, which could decrease the specific thrust. Furthermore, an increased compressor ratio would mean a change in the turbine geometry to handle the new load. For the burner, a change in the increased burner temperature would mean a change in the turbine material. These options are detrimental to time and budget. Any changes in the core of the engine have a high technical risk in terms of precision manufacturing, retaining pressure seals, and acquiring static and dynamic balancing.

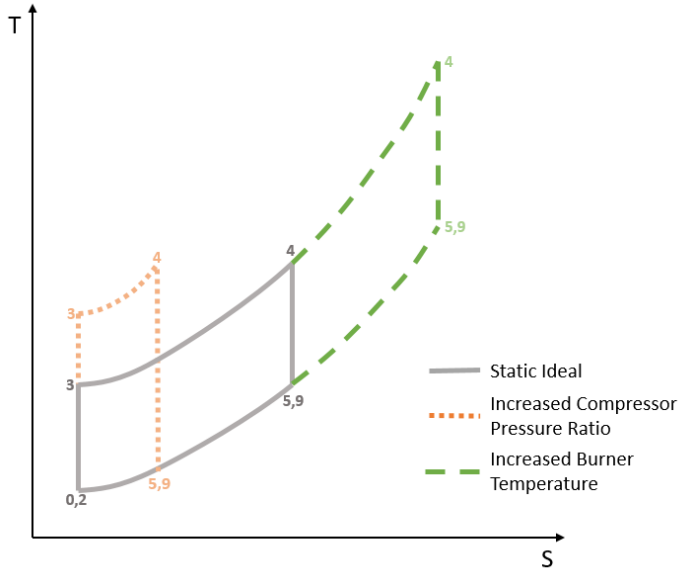

Figure 3. T-S Diagram

D. Addition of Afterburner

The fuel in a turbine engine burns in an excess amount of air, providing enough oxygen to support further combustion. Because of this effect, it is possible to inject additional fuel for burning downstream of the turbine, increasing the overall thrust of the engine. The difficulty, however, is anchoring the flame and maintaining its stability for the fuel to reignite. With the high temperatures during this process, material selection is critical due to thermal fatigue and material operating temperature limits. This new component could potentially add an undesirable amount of weight from the fuel delivery and flame holder.

E. Supersonic Nozzle

A supersonic nozzle could increase the exit velocity of the engine by using a converging-diverging configuration and accelerating the flow to supersonic speeds. However, an analysis is shown in Section IV using Figure 12 to illustrate why a supersonic nozzle is not possible for the JetCat P100 engine. The engine chamber pressure is not high enough to overcome the back pressure, which would be critical for reaching supersonic speeds. This low chamber pressure results from the compressor pressure ratio being a mere 2.9. The pressure ratio at the exit may not be sufficient to achieve supersonic flow. Furthermore, the turbine extracts energy from the flow exiting the combustor

and then expands it to reduce the total pressure. Therefore, the combustor would also have to be modified because they are interrelated.

F. Material Improvements

For weight reduction, specific components of the engine were weighed. The stated weight of the entire engine from JetCat is 1080 grams. The original nozzle weighed 61 grams, the starter cap 2 grams, and the engine inlet cowling 33 grams. Options for the inlet cowling modification were removal entirely, eliminating excess material, or using a lighter material. For the nozzle, weight was not the only characteristic under consideration, but material properties as well, due to the high exhaust gas temperatures. The current nozzle is made from a steel alloy, experiencing exit gas temperatures upwards of 1300 degrees F. Figure 4 shows three materials that were considered to manufacture the nozzle, based on operating temperature ranges, densities, and cost.

EGT:1292 F

Aluminum

Alloy	°C	°F
1100	640–655	1190–1215
2024	500–635	935–1 180
3003	640–655	1190–1210

Stainless Steel

Material	C	F
SS 304 alloy	1400	2550
SS 316 alloy	1300	2500

Titanium

Material	C	F
Titanium	1725	3135

*Densities
*Cost

42.64 g/cu. In.
$9/lb

131.08 g/cu. In.
$4/lb

73.906 g/cu. In.
$23/lb

Figure 4. Material Properties

The lightest material shown is an aluminum alloy with a density of 42.64 grams per cubic inch. However, the melting point is only 1200 degrees F, with an operability range a few hundred degrees lower. The exhaust gas temperature is too high for this material to handle. Stainless steel alloys can experience much higher temperatures, but the density is the highest of the three materials shown, resulting in the most weight. Finally, titanium not only has the highest melting point of 3100 degrees F and operating range upwards of 2800 degrees F, but the density is almost half that of stainless steel. However, the problem with this material is that titanium is almost six times more expensive than stainless steel and twice as costly as aluminum. Titanium was chosen of the three materials for its high-temperature operating range and low density.

III. Parametric Cycle Analysis

A. Parametric Cycle Analysis

Parametric cycle analysis (PCA) is commonly used in aircraft engine design to study the thermodynamic changes of air as it moves between each component within the engine. The inputs of the real PCA performed in this analysis include engine specifications given by the manufacturer, gaseous properties of air, and assumptions about component efficiencies which are based on similar engines and an assumed level of technology. For turbojet nomenclature and the T-S diagram, see Figure 5.

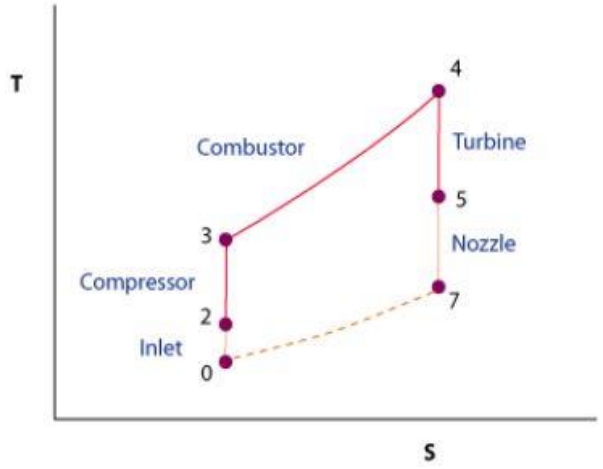

Figure 5. Turbojet T-S Diagram

With the goal of designing a new nozzle, a PCA was performed to predict the engine's theoretical maximum exit Mach number, and a mass flow parameter (MFP) analysis was performed to determine the optimal nozzle exit area to achieve this Mach number. For the PCA, the following assumptions were made:

- The airflow is approximately steady and 1-D.
- The air has a constant ratio of specific heats upstream of the burner, γ_c, and downstream of the burner, γ_t. These values were calculated based on estimated air temperatures and are tabulated in Table 1.
- The air has a constant specific heat upstream of the burner, Cp_c, and downstream of the burner, Cp_t. These values were calculated based on estimated air temperatures and are tabulated in Table 1.

Table 1. Specific Heat Values

γ_c	1.36
γ_t	1.4
Cp_c	211 lbf*ft/lbm*R
Cp_t	187 lbf*ft/lbm*R

- There is no power take-off from the engine shaft.
- Parameters not given by the manufacturer or solved for in the PCA are estimated using a level of technology corresponding with 1980s technology.
- The airflow is perfectly expanded at the nozzle exit.

The maximum exit Mach number was calculated by estimating the ratio of the total pressure to the static pressure at the nozzle exit. This ratio was found using the following equation,

$$\frac{P_{t_9}}{P_9} = \pi_r \pi_d \pi_c \pi_b \pi_t \pi_n \frac{P_0}{P_9}$$

Equation 2

in which π denotes the pressure ratio of a specified component. The pressure ratio for each component is given in Table 2.

Table 2. Component Pressure Ratios

Component	Pressure Ratio		Value	Assumption
Stream tube	π_r	P_{t0}/P_0	1	Static conditions
Inlet/diffuser	π_d	P_{t2}/P_{t0}	0.97	Level of technology
Compressor	π_c	P_{t3}/P_{t2}	2.9	JetCat Data
Burner	π_b	P_{t4}/P_{t3}	0.93	Level of technology
Turbine	π_t	P_{t5}/P_{t4}	0.64	Power Balance
Nozzle	π_n	P_{t9}/P_{t5}	1	

π_r is the ratio of the total pressure to the static pressure of the stream tubes entering the inlet. Because the engine will be tested in static conditions, this ratio can be assumed to be one. All other component pressure ratios are the ratios of the total pressure just downstream of the component to the total pressure just upstream of the component. The pressure ratios of the inlet and burner were estimated based on the assumed level of technology. The pressure ratio of the compressor was a value given by the manufacturer. The pressure ratio of the turbine was estimated using a power balance between the turbine and the compressor. The following equation represents this power balance:

$$c_{p_c}(T_{t_3} - T_{t_2}) = (1+f)\eta_{mech}c_{p_t}(T_{t_4} - T_{t_5})$$

Equation 3

The left side of the equation represents the energy given to the airflow in the compressor, and the right side represents the energy extracted from the airflow in the turbine. Using this equation, the ratio of total temperatures downstream and upstream of the turbine is known, and the turbine pressure ratio is calculated. The nozzle pressure ratio was initially assumed to be one, though a Rayleigh flow analysis and Fanno flow analysis would later be performed on the nozzle to predict losses more rigorously. Finally, P_0/P_9 was be estimated to be unity in accordance with the assumption of the flow being perfectly expanded at the nozzle exit. The total pressures and temperatures estimated at each engine station are mapped in the diagrams below.

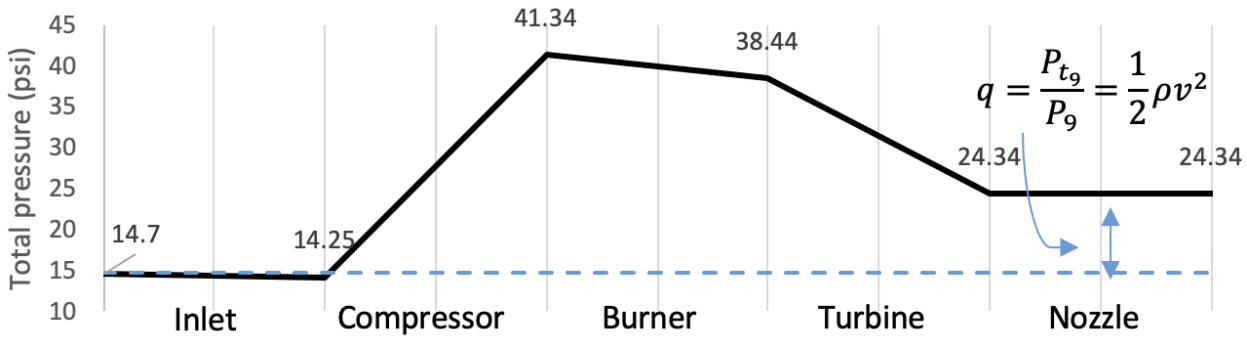

Figure 6. JetCat P100-RX Component Pressure Diagram

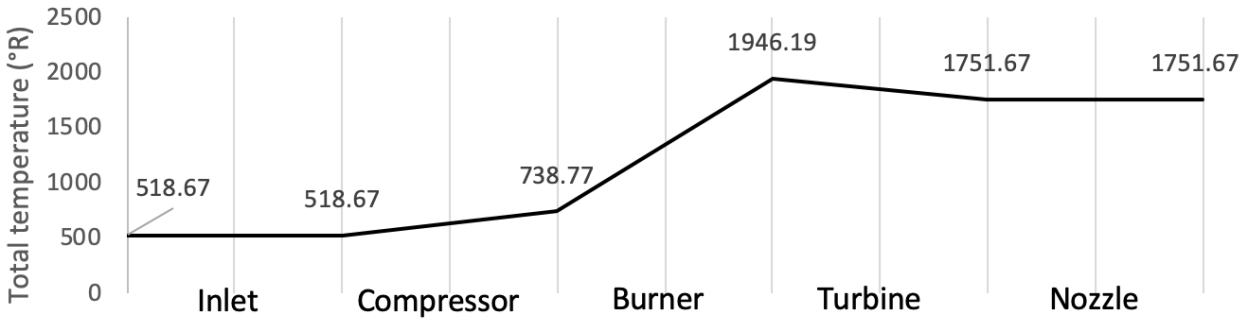

Figure 7. JetCat P100-RX Component Temperature Diagram

Knowing all component pressure ratios and multiplying them out, P_{t9}/P_9 was calculated. Based on P_{t9}/P_9, an exit Mach number and exit velocity were predicted. The following equations were used.

$$\frac{T_{t_9}}{T_9} = \left(\frac{P_{t_9}}{P_9}\right)^{\frac{\gamma-1}{\gamma}}$$

Equation 4

$$V_e = \sqrt{2c_p g_c (T_{t_9} - T_9)}$$

Equation 5

Next, a mass flow parameter (MFP) analysis was performed to estimate the necessary nozzle exit area to achieve the optimal Mach number that was found. The following equation was used,

$$MFP_9 = \frac{m_{dot_0}\sqrt{T_{t_9}}}{A_9 P_{t_9}}$$

Equation 6

in which MFP is a compressible flow function that depends on Mach number and ratio of specific heats. The results of the PCA are found in Table 3.

Table 3. PCA Results

Table of Results	
Parameter	**Value**
P_{t9}/P_9	1.656
M_9	0.895
V_9	1725 ft/s
A_9	2.108 in^2

The PCA results indicate an optimal exit velocity of 1725 ft/s which is considerably higher than the rated exit velocity of 1425 ft/s. This finding shows that the original nozzle design is not optimized and that a nozzle redesign is a feasible strategy for thrust improvement. The new nozzle was designed with a converging area to assist the engine in achieving the optimal exit Mach number found. It should be noted that the nozzle exit area A_9 calculated here does not consider boundary layer growth, which will be analyzed in the Fanno flow analysis. The exit area of the new nozzle will need to be slightly larger in this case.

B. Rayleigh Flow Effects

A Rayleigh flow analysis was performed to predict nozzle losses due to heat transfer. Heat transfer from the airflow can affect nozzle pressure losses as well as exit Mach number. This effect is of concern when the engine is throttling up because the nozzle has not reached thermal equilibrium yet. For this analysis, the following assumptions were made:

- No combustion reactions take place in the nozzle airflow. All combustion is completed in the burner.
- The nozzle is treated as a constant area duct.
- Friction is negligible.

The following equation governs Rayleigh flow and is visualized in the accompanying diagram.

$$\frac{dP_t}{P_t} = -\frac{\gamma M^2}{2}\frac{dT_t}{T_t}$$

Equation 7

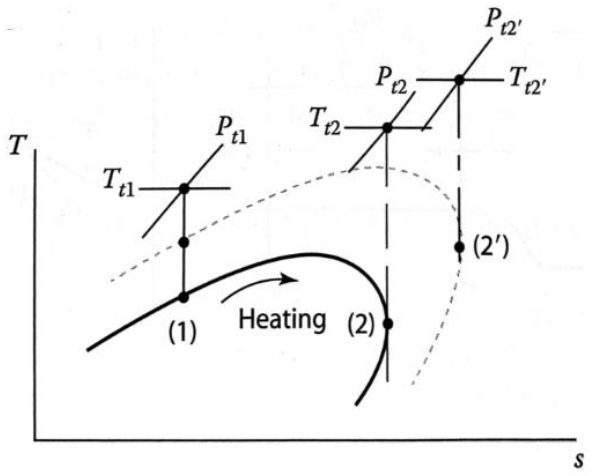

Figure 8. Rayleigh Flow T-S Diagram[1]

The diagram shows a typical Rayleigh line, with subsonic flow taking place above point (2) and supersonic flow taking place below point (2). It is noted from the diagram that for subsonic flow, an increase in the total temperature of the Rayleigh flow causes a decrease in total pressure and vice versa. If the subsonic airflow loses heat energy through the nozzle under Rayleigh conditions, the flow is expected to have an increase of total pressure and a decrease in Mach number. To further explore the effects of heat loss on total pressure, the Rayleigh equations were iterated in GASTAB using different combinations of Mach number upstream and downstream of the nozzle. Tables 4 and 5 below show total temperature losses and corresponding nozzle pressure ratios for each of these combinations. Values highlighted in green represent the best-case scenario, values in red represent the worst-case scenario, and values in grey are implausible due to the necessity of heat addition.

Table 4. Rayleigh Flow Temperature Difference

Temperature Difference (R)					
M9	M7				
	0.7	0.75	0.8	0.85	0.89
0.6	-195.376	-264.626	-317.032	-353.666	-375.109
0.65	-82.672	-147.915	-197.287	-231.801	-252.003
0.7	0.000	-62.303	-109.450	-142.409	-161.701
0.75	60.163	0.000	-45.529	-77.356	-95.985
0.8	103.015	44.375	0.000	-31.021	-49.179
0.85	131.704	74.085	30.481	0.000	-17.842

Table 5. Rayleigh Flow Nozzle Pressure Ratios

Pi_n					
M9	M7				
	0.7	0.75	0.8	0.85	0.89
0.6	1.030	1.043	1.054	1.063	1.068
0.65	1.014	1.027	1.038	1.046	1.052
0.7	1.000	1.013	1.023	1.032	1.037
0.75	0.988	1.000	1.010	1.019	1.024
0.8	0.977	0.990	1.000	1.008	1.013
0.85	0.969	0.982	0.992	1.000	1.005

The worst-case scenario shown is a 375 °R temperature drop through the nozzle, which corresponds to a nozzle pressure ratio of about 1.068. Even with such a drastic decrease in Mach number and total temperature, the nozzle pressure ratio would only be about 7% higher than the original assumed nozzle pressure ratio, and the nozzle is not expected to extract that much heat from the flow. Therefore, Rayleigh losses can be considered negligible.

C. Fanno Flow Effects

A Fanno flow analysis was performed to predict nozzle losses due to friction. For this analysis, the following assumptions were made:

- No combustion reactions take place in the airflow in the nozzle. All combustion is completed in the burner.
- The nozzle is treated as a constant area duct.
- Heat transfer is negligible.

The primary influencing factor in Fanno flow is the nozzle friction coefficient, c_f. For this analysis, c_f was estimated to be 0.021 based on its Reynold's number and material, and it is the worst-case scenario. Mach number at the entrance of the nozzle was assumed to be 0.89. Similar to with the Rayleigh flow analysis, GASTAB was used to run the Fanno flow equations. Using the coefficient of friction, entrance Mach number, and known duct length, the nozzle pressure ratio was calculated to be 0.97 under Fanno conditions, only a 3% difference from the original assumed nozzle pressure ratio. Therefore, friction effects can be considered to have a negligible effect on the nozzle pressure ratio.

Next, a new nozzle exit area was calculated to account for the boundary layer caused by friction. To account for this effect, a discharge coefficient was estimated from the nozzle half angle, which is 10°.

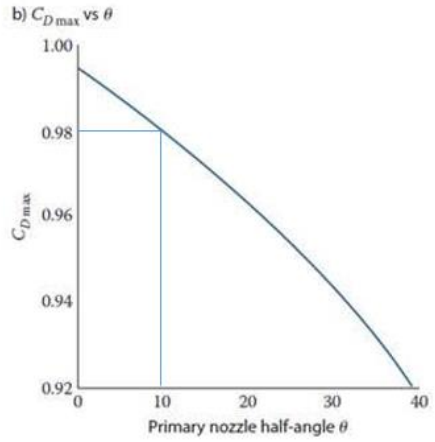

Figure 9. C_{Dmax} vs θ

Based on Figure 9, the discharge coefficient was estimated to be 0.98. Using this discharge coefficient, the new nozzle exit area was calculated to be 2.154 in^2.

IV. Nozzle Geometry Analysis

A cross-sectional view of the original nozzle geometry is shown below in Figure 11. The nozzle has an inlet area of 2.51 square inches and an exit area of 2.76 square inches. The nozzle has a rounded cone in the center to keep the flow from diffusing at the outlet of the turbine and to guide the flow out of the nozzle. Upon further analysis, it is clear that the current nozzle is not the optimal nozzle geometry for the engine. Figure 10 shows a cross-sectional view of the nozzle effective area seen by the airflow, without the rounded cone. The effective area is constant until the rounded inner cone begins to taper down as well as the exterior. Once the rounded cone ends, the effective area increases rapidly and then decreases as the nozzle outer wall continues to taper down.

Figure 10. Original Nozzle

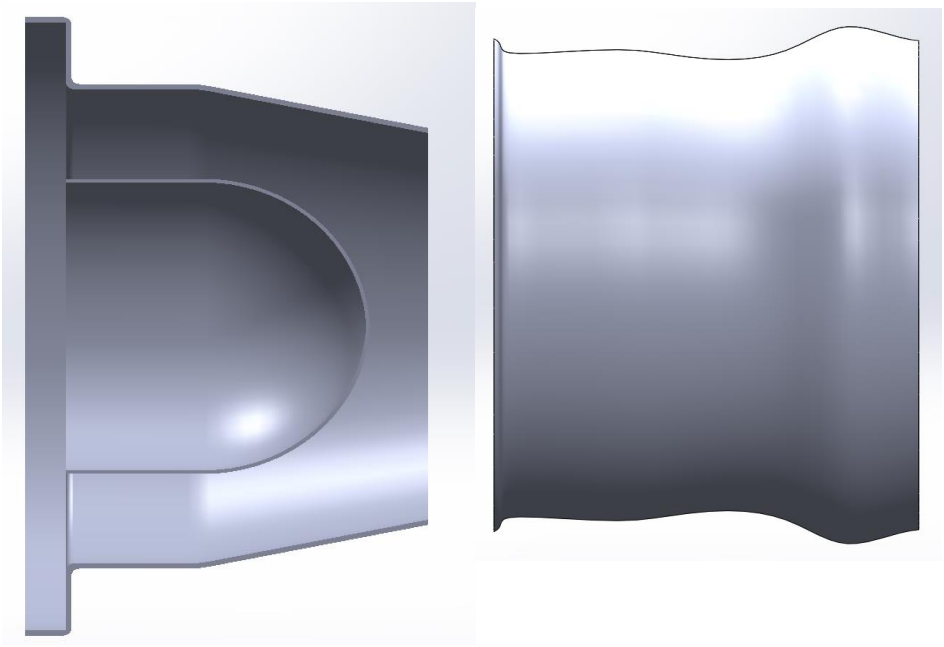

Figure 11. Original Nozzle Geometry (Left) and Effective Flow Area (Right)

The exit area of the original nozzle is 2.76 square inches, which is larger than the inlet area of the nozzle. This nozzle is effectively a diffuser and therefore slows down the air. This exit area was identified as a thrust improvement area, as, recalling from Equation 1, an increase in V_9 causes an increase in thrust. Initially, a supersonic nozzle option was evaluated. However, this change is not possible for the current turbine exit pressure. Since the compressor pressure ratio is only 2.9, the chamber pressure is not high enough to allow for exit flow characteristics

which can create a supersonic flow with a converging-diverging nozzle. As shown in Figure 12 below, the JetCat exit flow follows line 3 in the graphs based on the turbine exit total pressure. If the nozzle had been designed as a converging-diverging nozzle to reach supersonic flow, some outside force would have to be applied to increase the total pressure exiting the turbine. If not, the atmospheric pressure would cause a back pressure in the nozzle and choke the flow, represented by lines 4.1 4.2 and 4.3 in Figure 12. Therefore, because of the design of the compressor, this engine is constrained to subsonic flow conditions through the nozzle.

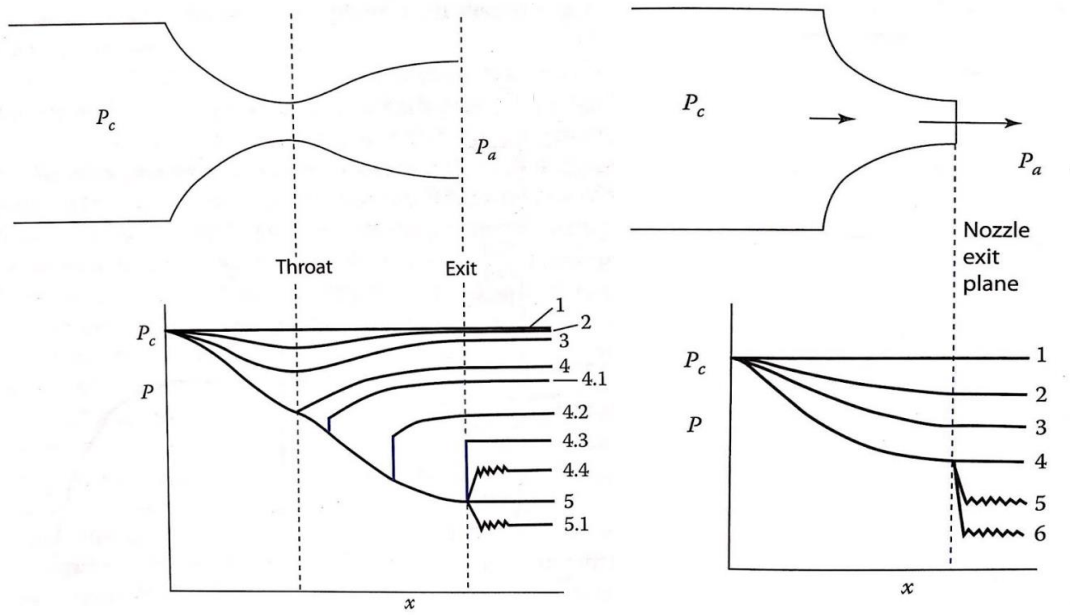

Figure 12. Converging-Diverging Nozzle (Left) and Converging Nozzle (Right) Pressure Diagrams[1]

Instead, a new, converging nozzle was optimally designed to increase the exit velocity of the engine. From the parametric cycle analysis (PCA), it was found that the maximum possible exit Mach number is 0.89. For the rated engine mass flow rate, this velocity correlates to an exit area of 2.152 square inches. In order to reach this exit area, a new nozzle outer geometry and new inner cone were designed. The nozzle cross-section is shown in Figure 13.

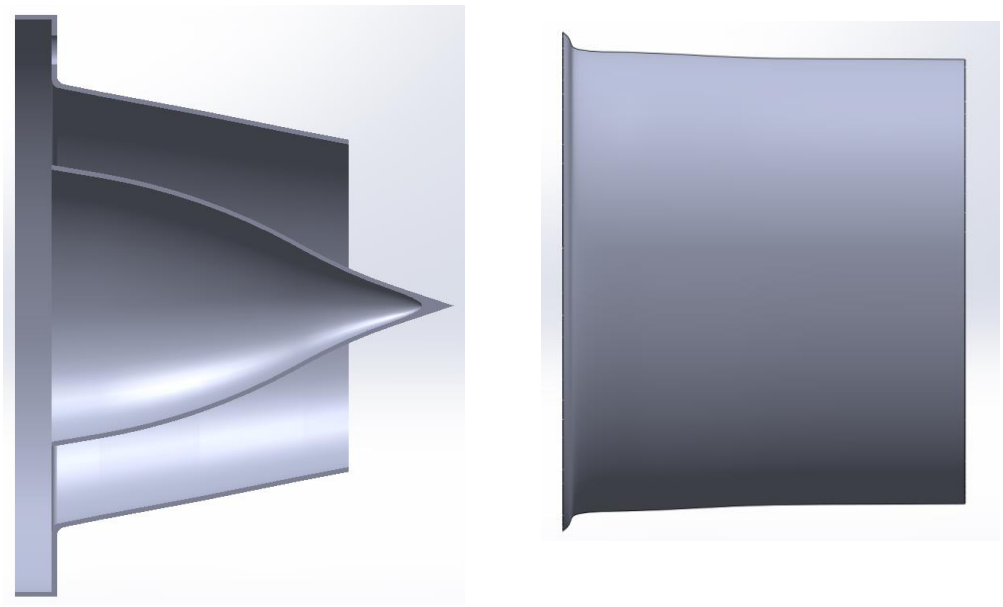

Figure 13. New Nozzle Geometry (Left) and Effective Flow Area (Right)

The design of the cone allows the flow to remain attached throughout the entire length of the nozzle. The nozzle was designed in CAD using a spline method where the angle between any two concurrent points does not exceed 10 degrees. Furthermore, since the cone comes to a point rather than a rounded edge as designed by JetCat, it mitigates flow recirculation that was assumed to reduce thrust. The angle that the flow sees begins at 10 degrees before turning inward up to 30 degrees then back out to 20 to ensure that the flow off the inner cone stays attached. The new nozzle is 3-D printed out of titanium, which has several benefits for this application: the density of titanium is much lower than steel. This improvement allowed for a reduction of 31 grams. Titanium also has a much higher operability range in terms of temperature, ideal for withstanding the heat from the exhaust gas.

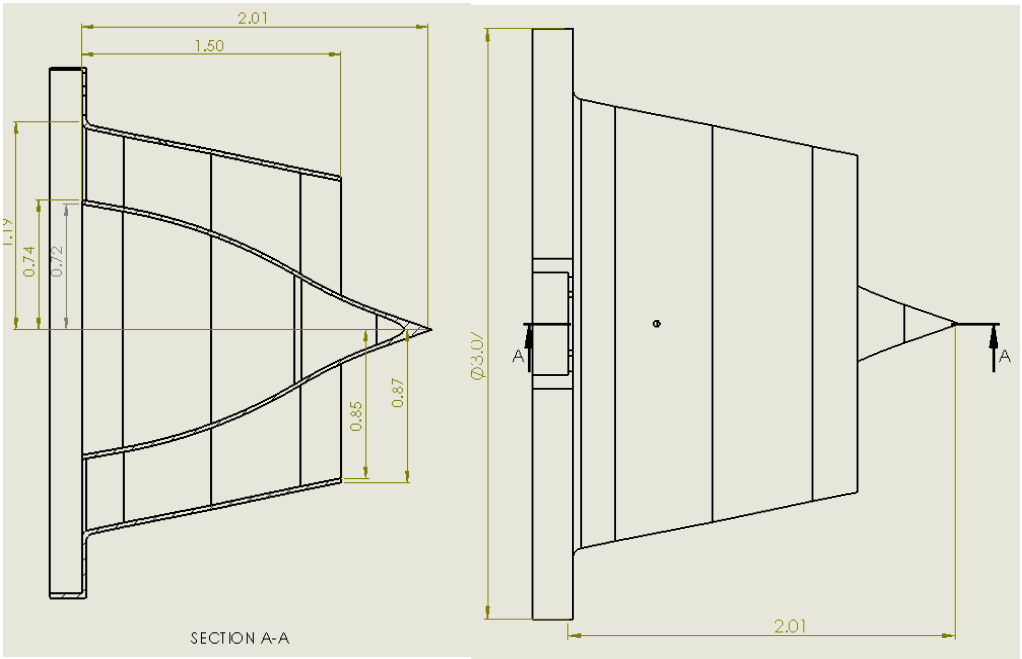

Figure 14. New Nozzle Schematic

V. Experimental Setup and Procedures

A. Setup

All tests were performed at the Oklahoma State Advanced Technology and Research Center (ATRC) wind tunnel. In order to conduct experiments, the engine would be mounted on a thrust stand and placed in an open loop 3x3 ft. section. This thrust stand features a moment arm and an integrated load cell both of which are used to obtain thrust data. Additionally, the engine control unit, fuel pump, batteries, and other components necessary to successfully run the engine can be mounted on the cage surrounding the thrust stand.

Another feature of the wind tunnel is a five-hole probe which is used to determine the direction and magnitude of velocity as the flow exits the nozzle. In order to withstand the high exhaust gas temperature leave the nozzle, the probe was constructed with Inconel. The probe is also mounted on a traverse to allowing for movement of the probe along the x-y plane. During testing runs, the data collected is logged by an air data computer connected to the probe.

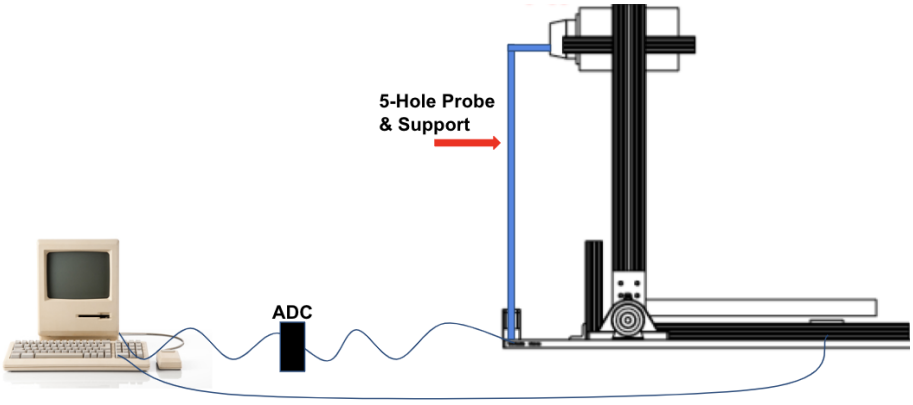

Figure 15. 5-Hole Probe and Load Cell Setup

B. Procedures

The main requirements for the 5-hole probe apparatus includes accurate data reading from the probe and load cell which was a driver for the experimental setup and instrumentation calibration. A desktop and air data computer were required to record data and interpret signals. The major risk to the integrity of the experiment was the possibility of the 5-hole probe deflecting in the axial direction due to the force caused by the high exhaust gas velocity of at least 971 mph. This risk was minimized by constructing a mount that held the probe to the test stand.

Figure 16. 5-Hole Probe

Figure 17. Thrust Stand in Wind Tunnel

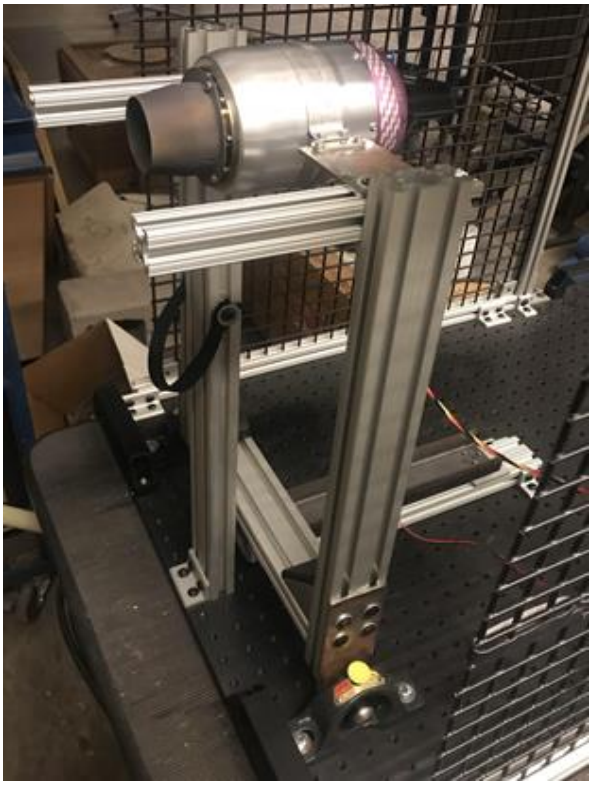

Figure 18. Engine secured in Thrust Stand

The engine was mounted on a custom-built test stand. The test stand was configured with an integrated load cell and placed in the wind tunnel. The load cell took thrust readings and fed the data to a computer where it was logged. The 5-hole probe was mounted on a traverse which allowed for it to be moved precisely in a plane parallel to the nozzle exit plane. The probe fed data into the air data computer which then got logged and interpreted on the desktop.

VI. Exit Guide Vanes

Thrust is maximized when the airflow out of the nozzle is directed fully in the axial direction. However, due to rotating turbomachinery, the airflow in an engine will typically have swirl, especially downstream of the turbine, resulting in a loss in thrust. In order to redirect the flow in the axial direction, exit guide vanes were designed. The 5-hole probe was used to create a rough swirl profile of the engine with the original nozzle. The swirl profile is pictured below.

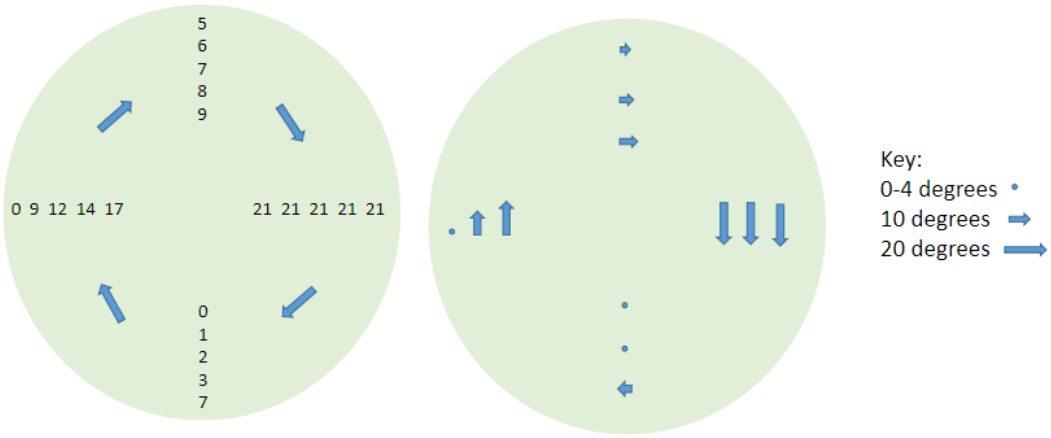

Figure 19. Swirl Profile (Degrees)

The swirl data for the right side of the nozzle exit plane was ignored since all values were maxed out. This abnormality could have been caused by the positioning of the five-hole probe relative to the support posts in the nozzle. Additionally, swirl values closer to the hub were given less weight than swirl values near the tip because the higher swirl values near the hub could have been influenced by flow recirculation caused by the rounded nub. It was determined that the airflow was seeing anywhere from 5 to 15 degrees of swirl, depending on location on the exit plane, which would later be used to decide the angles of the exit guide vanes to be printed.

To design the exit guide vanes, several variables were considered. The variables included solidity, axial position, turning angle, vane number, and airfoil shape. Some of these parameters were design decisions and some were decided by experimentation and cost/benefit analysis. The axial position of the guide vanes was chosen to be directly behind the turbine exit. This decision was made because, historically, this location is where exit guide vanes are placed on commercial engines. Seven guide vanes were chosen based on weights. With too many vanes, weight is too high and chord length is too small, but with too few vanes, chord length is too long and again weight is too high. The decision on number of exit guide vanes was chosen in conjunction with solidity calculations. Solidity is a measure of the spacing of the exit guide vanes divided by the vane chord length, meaning that the higher the solidity, the more they will straighten out the flow; a constant chord length was chosen instead of a constant solidity. This decision caused a variance in solidity from the leading to the trailing edge ranging from 1 to 0.66 with the solidity remaining higher at the hub where the angularity of the flow is highest. The solidity of one was chosen as an optimal solidity to have enough effect on the flow to straighten out the flow but not to be so high that the weight of the guide vanes was undesirable. Finally, the airfoil shape was chosen based upon the flow angle hitting the leading edge of the vanes.

The number of vanes in each configuration tested was determined based on a weight and length analysis. When analyzing the number of vanes, prime numbers were chosen because of their ability to damp out vibrations and reduce flow shedding interference between vanes. A weight analysis was done on the different vane configurations in order to understand what the optimal configuration was for the lowest weight. This analysis showed that higher vane configurations were lighter than lower vane configurations, due to their shorter length and lower thickness. For this reason, the lowest vane configuration of three was rejected due to length and higher vane configurations were rejected due to a lack of structural integrity. A representation of the length of the 3-vane configuration blade and 23 vane configuration blades are shown in Figure 20.

Figure 20. 3 Vane Config. Blade vs 23 Vane Config. Blade

Table 6. Design Choices

Design Choices	
Constant chord length	0.687 inches
Number of Vanes	7
Solidity (hub, tip)	1, 2/3
Airfoil	NACA 0012
Angle	5, 10 degrees

The two vane configurations chosen for printing have flow turning angles of 5° and 10°, both with 7 guide vanes. This guide vane configuration was selected as it was deemed a balance between weight and structural integrity. The angles were chosen based on the swirl data collected using the original nozzle. In addition to these two prints, another design with the new nozzle geometry and 3 support posts was also printed to test the effect of the new geometry without the effect that the guide vanes. The best flow turning angle were chosen from the experimental results. A CAD model of these two configurations are shown in Figure 20.

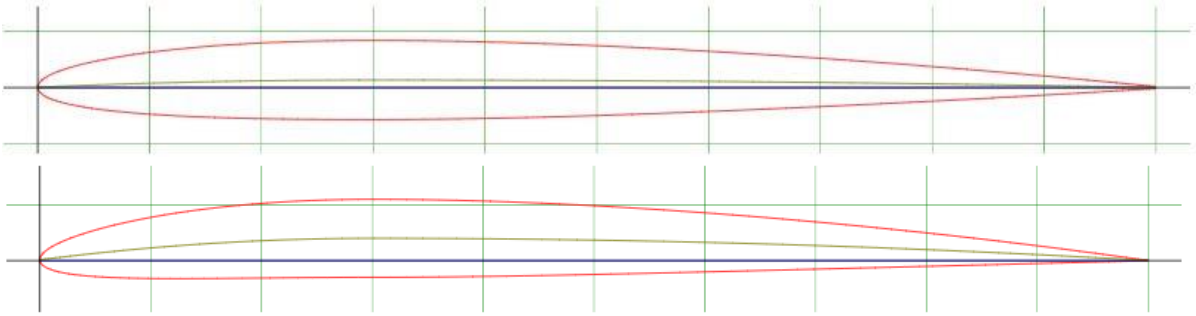

Figure 21. 5- and 10-Degree Airfoils

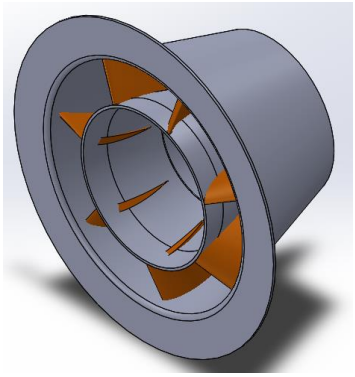

Figure 22. 7-Guide-Vane Configuration

VII. Results

A. Nozzle Geometry

To evaluate the improvement made by the new nozzle geometry alone, the new nozzle with no guide vanes was tested. This nozzle had three posts attaching the inner cone, similar to the original JetCat designed nozzle. Thrust tests were performed using the load cell, which yielded a 3.42 lbf improvement in thrust from the original nozzle, which is an 18.3% thrust increase. When considering the reduced weight of this new nozzle, the-thrust-to- weight ratio increased by 22%. The nozzle geometries are shown below in Figure 23.

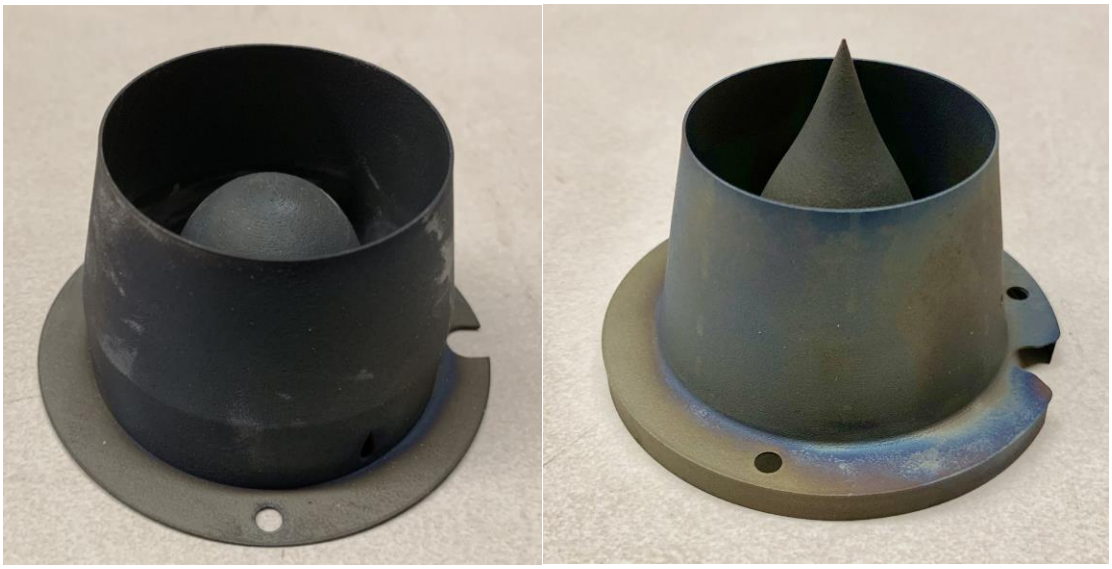

Figure 23. Original Nozzle Geometry (Left) and New Nozzle Geometry (Right)

B. Exit Guide Vanes

To evaluate the improvement made by the exit guide vanes, thrust tests were run using the new nozzle geometry with the addition of both 5 degree and 10-degree guide vanes. The nozzle with the 5-degree guide vanes increased the thrust by another 1.43 lbf from the new nozzle geometry test with no guide vanes, an improvement of 5%. The nozzle with the 10-degree guide vanes increased the thrust by another 1.76 lbf from the new nozzle with no guide vanes, an improvement of 3.8%. Based on these results, the nozzle with the 10-degree guide vanes gave approximately 0.33 lbf more thrust than the nozzle with 5-degree guide vanes, and it had a slightly greater improvement in thrust to weight ratio. Next, the five-hole probe was used to create a swirl profile for the nozzles with 5 degree and 10-degree guide vanes, and these swirl profiles were compared to the swirl profile of the original nozzle in order to analyze the effectiveness of the guide vanes in taking out swirl. The swirl profile of all three nozzles is pictured below.

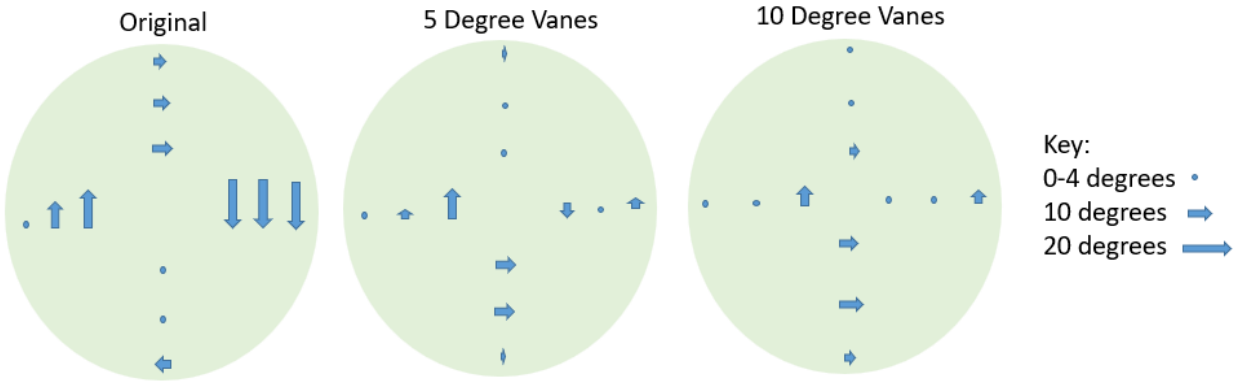

Figure 24: Swirl Results of Original Nozzle and Nozzles with Guide Vanes

It is clear from the representation of swirl shown above that the decrease in swirl from the original to the 5-degree guide vane configuration is significant, especially in the horizontal readings. This finding reflects what was found in the thrust tests. Comparing between the 5 degree and 10-degree configurations, a slight reduction in swirl can be

seen. For this reason, along with thrust test results, the 10-degree configuration was chosen as the final guide vane design for the nozzle.

C. Material Weight Savings

To evaluate the weight savings made by changing the material of the nozzle, the old and new nozzles were weighed, and the results compared. The original nozzle for the JetCat P100 weighed a total of 60.7 grams and was comprised of steel, whereas the final nozzle design with seven 10-degree guide vanes weighed a total of 29.5 grams and was 3D printed out of titanium. This change allowed for an overall weight improvement of 2%.

VIII. Inlet Cowling Improvement

The original inlet cowling is made of aluminum and weighs 33 grams. This inlet cowling leaves a significant amount of improvement in weight reduction. Tests were initially conducted to evaluate any thrust effects from running the engine without an inlet cowling, however thrust decreased noticeably: by about 0.2 lbf. Therefore, for an inlet cowling of different material, several options were evaluated: 3D printed in plastic, a carbon fiber and epoxy layup, and sanded foam.

The best option in terms of weight was chosen to be foam, which was formed through using a CNC machine and then sanding down the foam to fit onto the compressor inlet. The final foam inlet cowling weighs 1 gram, creating a weight reduction of 32 grams total; after running thrust tests, no thrust reduction was seen.

Figure 25. Original Inlet Cowling (Left) and New Inlet Cowling (Right)

IX. Battery Improvement

Opportunity for weight reduction was seen in the battery that powers the Engine Control Unit as well. The original battery weighs 200 grams. The battery is a 9.9 V, 3 cell, 2100mAh battery; voltage and cell count cannot be increased or decreased when changing batteries for the ECU because it only runs with a certain amount of power. However, the milliamp hours of the battery can be changed in an RC setup; this parameter controls the amount of time the battery can run. RC hobbyists will often use batteries of differing milliamp hours in order to increase endurance or decrease weight. A 2100 mAh battery weighing 170 grams was ordered, along with a 1600 mAh battery weighing 110 grams. The engine ran with the new 2100 mAh battery for its full throttle, 1-minute run successfully. However, the engine would not complete the startup sequence when the ECU was connected to the 1600 mAh battery, as the engine enacted the failsafe to shut down the engine. Due to this failsafe mode, the lighter 2100 mAh battery was chosen for the final engine configuration.

X. Conclusions

As a result of all modifications made to the engine and system, the thrust-to-weight ratio of the engine improves from 6.64 to 8.75. The original weight is 1280 grams, with a measured thrust of 18.7 lbf whereas the improved engine design produces a measured thrust of 23.02 lbf and a weight of 1193 grams. Table 7 below show the

percent change in thrust and weight of each modification made to the JetCat P100 engine, as well as the overall thrust-to-weight percent improvements.

Table 7

Component	Thrust Improvement	Weight Change
Exit Guide Vanes	(+) 1.23 lbf	(+) 0.41 g
Nozzle Geometry	(+) 3.58 lbf	(-) 31.2 g
Cowling Redesign	0 lbf	(-) 32 g
Battery Substitution	0 lbf	(-) 30 g
Total	(+) 4.81 lbf	(-) 92.8 g

To help visualize this impact, the bar graph below shows the percent change created from each improvement in the engine. A majority of the improvement in thrust results from the change in nozzle geometry, while the improvements in weight are evenly resulting from the nozzle, inlet cowling, and battery improvements. The final thrust-to-weight ratio improvement was 32%, a considerable improvement from the original JetCat design.

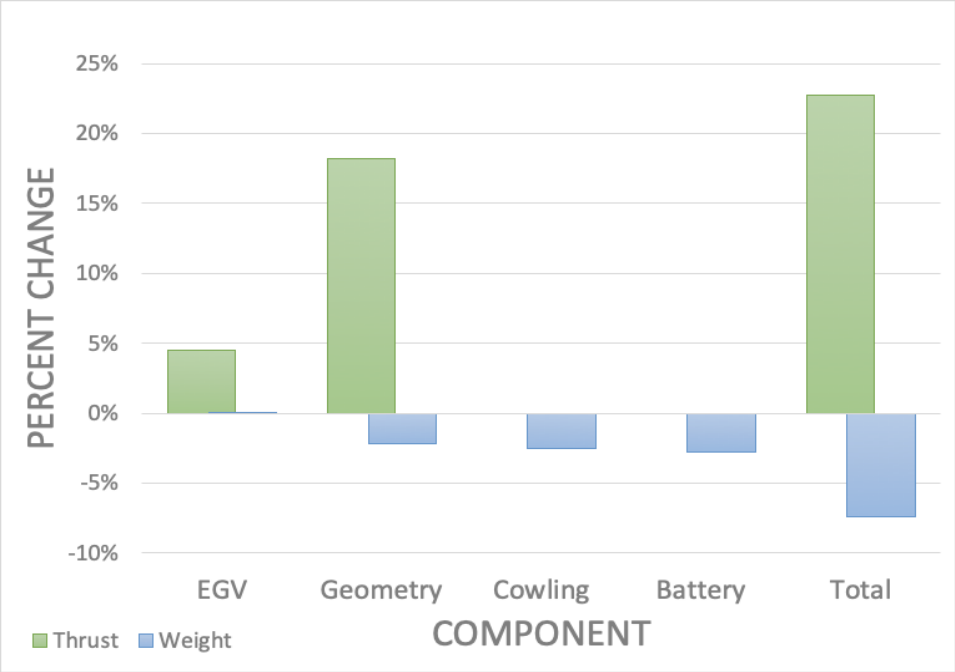

Figure 26: Percent change of thrust and weight for modified components

References

[1]Mattingly, J. D., and Boyer, K. M., *Elements of Propulsion: Gas Turbines and Rockets*, Reston, VA: AIAA, 2016.